Monitoring of the absolute water content in porous materials based on embedded humidity sensors

Christoph Strangfeld[a,*], Sabine Kruschwitz[a,b]

[a] *Bundesanstalt für Materialforschung und -prüfung, Unter den Eichen 87, 12205 Berlin, Germany*
[b] *Technische Universität Berlin, Gustav-Meyer-Allee 25, 13355 Berlin, Germany*

Abstract

Moisture transport monitoring may indicate the onset of deterioration in porous building materials prior to damage occurring. Most moisture measurement systems provide only qualitative values, require extensive calibration, or are destructive. Thus, non-destructive and calibration-free monitoring systems are required. Our approach of moisture monitoring is to embed sensors that measure the relative humidity. In our experiment, screed samples are monitored during the hydration and evaporation process. Every test sample is equipped with 10 embedded sensors which measure the relative humidity across the thickness. Based on Hillerborg's approach, the relative humidity is converted into the corresponding pore saturation. In our study, the free water is computed without knowledge of the sorption isotherm. The free water is predicted and validated. The predicted weight decrease corresponds conclusively to gravimetrically measured weights. The embedded sensors yield the absolute liquid water content and enable an experimental, non-destructive monitoring of liquid water in porous materials.

Keywords: moisture monitoring, screed, Kelvin equation, embedded sensors

*Corresponding author
Email addresses: christoph.strangfeld@bam.de (Christoph Strangfeld), sabine.kruschwitz@bam.de (Sabine Kruschwitz)

1. Introduction

Moisture and moisture transport in concrete are important factors affecting the durability of concrete. Temperature gradients, mass transfer, and ion migration are mainly influenced by the free liquid water in the capillary system in porous materials. Thus, several chemical reactions leading to deterioration of our infrastructure are caused or highly accelerated due to moisture. In case of corrosion, free liquid water is a required reactant which further reduces the electrical resistance of concrete [1, 2]. The alkali-silica reaction is also promoted by free liquid water [3]. If cracks already exist, freeze-thaw cycles of water may immediately damage the concrete structure. Modern infrastructure objects like bridges, highways, tunnels, foundations, etc. are mainly built of reinforced concrete. Thus, almost the entire infrastructure is exposed to these deteriorations. For example, in Germany annual costs for repair and replacement are more than 13 billions Euro to maintain the status quo. Thus, a secure, powerful, and cost-efficient infrastructure mainly relies on early and accurate detection of hazardous moisture.

Although the exact knowledge of the amount of free liquid water in concrete is a crucial parameter in structural health monitoring, universal non-destructive methods to quantify moisture are missing so far. Thus, in practice, generally a two-stage approach is conducted. First, non-destructive devices based on resistivity or capacity measurements are used to measure the moisture distribution qualitatively. Then, at distinct spots, destructive moisture measurements like calcium-carbide method or Darr drying are performed. These tests are destructive, time-consuming, and provide only a point information. Furthermore, spatial moisture gradients or temporal varying moisture distributions are not recorded. Thus, experimental moisture monitoring is not feasible although it is crucial for most mass transfer processes. In the laboratory, approaches of moisture monitoring based on embedded electrodes [4] or embedded time domain reflectometry sensors [5] are elaborated. By means of calibrations, the sensor systems measure the moisture quantitatively. However, the calibration is com-

plex, highly time-consuming, and only valid for one distinct material under one distinct environmental condition. Hence, a transfer into the field is impossible or associated with a high measurement uncertainty.

Another approach to quantify the free water is based on the measurement of the humidity [6]. The free liquid water content in porous materials correlates with the equilibrium moisture content. Thus, humidity measurements in boreholes [6], crushed material samples, or via embedded sensors are performed [7, 8, 9, 10]. By applying the sorption isotherms and scanning-isotherms, the humidity values are converted directly into moisture [11]. Nevertheless, experimental determination of the sorption isotherm is costly, only feasible for one distinct material and the process may take months. Several models and simulations exist to approximate sorption isotherms [12]. Nevertheless, most models still require semi-empirical material parameters such as permeability, diffusivity, or conductivity.

Hillerborg [13] extends the well known Brunauer-Emmett-Teller (BET) theory [14]. In contrast to the BET theory, Hillerborg considers non-flat surfaces as well. Therefore, he adapted the Kelvin equation to absorbed water layers inside cylindrical pores. The two input parameters, pore radius and relative humidity, determine the saturation of a pore. Chaube et al. [15] uses Hillerborg's approach to predict the water release of a reference concrete block. The agreement between experiments and theoretical predictions are satisfying. Based on this work, Ishida et al. introduced the so-called inkbottle effect to predict the entire sorption isotherm, including the hysteresis between absorption and desorption. This approach is extended to non-isothermal conditions [16]. However, the investigated test samples have a size of 4 cm x 4 cm x 16 cm and have to completely reach the equilibrium moisture content to take a measurement [17]. Thus, the measurements take approximately two years and only a total weight loss is determined. Other researchers used Hillerborg's approach to predict other parameters, for example, the shrinkage of concrete in an early age of hydration [18], or to validate simulations of moisture transport models [19].

Although several studies show the high potential of Hillerborg's approach, the

analyses so far only result in an averaged moisture content for concrete blocks. However, advanced monitoring systems in civil engineering as well as complex mass transfer models for porous materials require a high spatial and temporal resolution of the moisture distribution. To fill this gap, we used embedded humidity sensor arrays of 10 sensors in 16 different screed samples. During hardening and drying, the humidity inside the samples was monitored. Based on the humidity profiles, the absolute free liquid water content is predicted with a spatial resolution of 0.1 mm for more than 300 days. Hence, the weight loss is calculated and experimentally validated by means of a high precision balance. The agreement between experiment and prediction proves the concept of quantifying the absorbed liquid water based on the adaption of Hillerborg's theory. Furthermore, this approach of measuring the relative humidity is independent of any calibration for the used materials. The sorption isotherm is no longer required, on the contrary, the sorption isotherm may be predicted based on this approach.

2. Free liquid water calculation in porous materials

In cement paste and screed, the moisture transport occurs in the pore system of the material. The mass balance adapted to moisture in porous materials describes the transport process. Thereby, a thermodynamic equilibrium between the free liquid water in the pores and the water vapour partial pressure is assumed. Equation 1 quantifies the moisture transport.

$$\frac{\partial \Theta}{\partial t} + \mathrm{div}(J) + Q \quad \equiv \quad 0 \tag{1}$$

The mass balance consists of three general terms. Θ is the mass of moisture in a unit volume of the considered materials in kg/m^3. The time derivation of Θ expresses the total water adsorption or desorption over time. The second term represents the spatial evolution of the moisture flux J in kg/m^{2}s. With $\Theta = \rho_l \phi s(r,h)$, Θ is replaced by the density of water ρ_l in kg/m^3 and the degree of pore saturation s and the pore volume distribution ϕ. Under isotherm and

isobar conditions, the pore saturation itself depends only on the pore radius r in nm and the relative humidity h in rH. The contribution of water vapour to the pore saturation is neglected in the current formulation. Equation 2 quantifies the pore saturation for cylindrical pores which relates the total volume of a pore to the water volume inside this pore [13].

$$s = 1 - \left(\frac{r - t_a}{r}\right)^2 \qquad 0 \leq t_a \leq r \tag{2}$$

The thickness of the adsorbed water layer t_a in nm begins at the fringe of the pore. If the humidity increases, more water passes into the liquid state due to the increase of the water vapour pressure. The adsorbed water layer increases and the pore fills up which coincides with a higher pore saturation. Based on the theory by Hillerborg, the resulting water layer is calculated by means of equation 3 and 4 [13].

$$t_a = \frac{t_w h C}{(1 - \frac{h}{h_m})(1 - \frac{h}{h_m} + Ch)} \tag{3}$$

$$h_m = \exp(-\frac{\gamma M}{\rho_l R T (r - t_a)}) \tag{4}$$

C is a material constant related to the moisture diffusivity and adapted to cement based materials. t_w is the thickness of one monomolecular water layer in nm. R is the ideal gas constant in J/molK, T the temperature in K, M the molecular mass of water in kg/mol, and γ is the surface tension in N/m. During adsorption, the humidity, at which the air volume in the centre of cylindrical pore disappears, is the so called maximum humidity h_m. Equation 4 is based on the Kelvin equation and takes into account the variation of the vapour pressure due to the curved liquid-vapour interface at the inner layer [20]. Hence, every pore radius possesses an individual maximum humidity h_m.

For every pore radius, the saturation is known based on this approach. The capillary saturation S_{cp} is the summation of all pore saturation multiplied with the corresponding pore volume and the density of liquid water. Based on equation 5, the absolute water content is determined.

$$S_{cp} = \rho_l \int_{r_{min}}^{r_{max}} \phi s dr = \rho_l \sum_{r_{min}}^{r_{max}} \frac{\triangle V}{\triangle r} s \triangle r = \rho_l \sum_{r_{min}}^{r_{max}} s \triangle V(r) \tag{5}$$

In our experiments, the pore volume distribution is measured at discrete radii. Thus, the incremental given pore volume is defined as $\phi = \frac{\triangle V}{\triangle r}$ and the integral in equation 5 is substituted by a summation.

The given theory is able to predict saturation during adsorption. Nevertheless, the saturation depends highly on the moisture history [15]. Ishida et al. introduce the inkbottle effect for a connected pore system [21]. The theory takes into account the probability of entrapped water in larger pores. Assuming a perfectly random geometric connection between the pores of varying sizes, the probability of a fully saturated pore is f.

$$f = V_{r_c}/V_r \quad with\ r_c \leq r \tag{6}$$

The critical radius r_c at a given humidity is the maximum pore radius at which a pore remains fully saturated, determined by the thermodynamic equilibrium. V_{r_c} depicts the cumulated pore volume at the critical radius and V_r is the cumulated pore volume at the considered pore radius during desorption. The total entrapped water $S_{ink} = \int_{r_c}^{r_{max}} f\phi dr$ is the summation from r_c to the largest observed pore radius r_{max}. For an incremental given porosity, equation 7 quantifies S_{ink}.

$$S_{ink} \quad = \quad \rho_l \sum_{r_c}^{r_{max}} \frac{V_{r_c}}{V_r} \triangle V(r) \tag{7}$$

In the case of desorption, the total free liquid water S_{total} contained in the pore system is the summation of the capillary and entrapped water. Furthermore, the probability that entrapped pores, which are already completely filled, do not contribute to the capillary water is incorporated by the factor $(1 - f)$ in equation 8.

$$S_{total} \quad = \quad (1 - f)S_{cp} + S_{ink} \tag{8}$$

With this formulation of moisture transport in porous materials, the hysteresis between adsorption and desorption under arbitrary relative humidity history is computed.

3. Experimental setup

First, the screed samples and their storage in the climate chamber are discussed. Then, the embedded humidity sensors are considered in detail. Eventually, the pore size distributions are documented, determined by mercury intrusion porosimetry and gas adsorption.

3.1. Screed samples and ambient conditions

In the current study, four cement-based (CT) and four calcium-sulphate-based (CA) screed types are investigated during the hydration and evaporation process. The product names of the different types are listed in table 1. For each screed type, two samples, one of 35 mm and one of 70 mm thickness, are equipped with embedded sensors and tested non-destructively. All samples are cylindrical with an inner diameter of 300 mm and are sealed at the bottom and sides in order to ensure a symmetric moisture transport. The casings are polyvinyl chloride (PVC) sewage pipes with a wall thickness of 7.7 mm. A transparent polyethylene foil is used as bottom material. The foil itself is stapled directly on the PVC pipe and sealed with a polymer based sealant. The materials are chosen to minimise moisture diffusion through the casing or the foil. A floating screed floor construction is simulated by placing the samples on top of styrodur (20 mm), styrofoam (40 mm), and washed out concrete (40 mm). [1]

All screed samples are manufactured during one day. For each screed type, the water/cement ratio recommended by the producer is used. All weights are checked by a high precision balance before mixing. After concreting, the samples are covered and stored over night in the production room (at approx. 295 K). On the following morning, the samples are stored in a ventilated climate chamber at an ambient relative humidity of h =50% rH and an ambient temperature of

[1] product name of the used screeds in the order of table 1: Weber.floor 4060, Weber.floor 4065, Weber.floor 4341, Sakret Beton/ Estrich BE, Knauf FE 25 A Tempo, Knauf FE 50 Largo, Knauf FE 80 Allegro, Weber.floor 4490

binder	type	compressive strength	bending tensile strength	water demand
cement	rapid screed	40 N/mm^2	7 N/mm^2	0.088 l/kg
cement	rapid heated screed	40 N/mm^2	6 N/mm^2	0.08 l/kg
cement	floating screed, fiber reinforced	20 N/mm^2	5 N/mm^2	0.135 l/kg
cement	concrete screed	35 N/mm^2	5 N/mm^2	0.11 l/kg
calcium-sulphate	floating screed	30 N/mm^2	6 N/mm^2	0.175 l/kg
calcium-sulphate	floating screed	25 N/mm^2	5 N/mm^2	0.163 l/kg
calcium-sulphate	floating screed	30 N/mm^2	6 N/mm^2	0.169 l/kg
calcium-sulphate	floating screed	25 N/mm^2	5 N/mm^2	0.15 l/kg

Table 1: Classification of the used cement-based and calcium-sulphate-based screed types

T =296 K. The storage of the samples in the climate chamber and the evolution of the ambient conditions in the climate chamber are shown in [10].

3.2. Measurement systems and embedded humidity sensors

Figure 1 presents the setup of the embedded sensors. The wired temperature and relative humidity arrays consist of ten individual sensors in the thick samples and five sensors in the thin samples [22]. The temperature sensors are MCP9700A three-pin thermistors in surface mounted device (SMD) design. They are installed directly on the board and all are covered by epoxy resin. The relative humidity sensors HIH-5031 are in SMD design as well. Within the range of 11% rH$\leq h \leq$ 89% rH, the humidity sensor HIH-5031 has a declared accuracy of $\pm$3% rH, including interchangeability. Below 11% rH and above 89% rH, the accuracy amounts to $\pm$7% rH including a reversible hysteresis of 3% rH. The overall repeatability for one single sensor is declared with 0.5% rH based on the data sheet. The sensors are mounted on the board and then placed in the orange casing. Thereby, the casing fulfils two tasks. On the one hand, each sensor gets its own separated housing inside the casing. This inhibits any air or moisture convection through the array. On the other hand, the casing positions the sensors directly behind the quartz glass filter. These filters are necessary in order to prevent direct contact of the humidity sensor membrane from water and screed mixture during concreting. The open area of the filter is 3.3 mm times 7.3 mm. Thus, the measured humidity is the average over this area. The centre of the filter is considered as the representative measurement position. The backside of the casing is also covered with epoxy resin. The humidity sensors are placed at vertical distances of 6 mm and the lowest humidity sensor is 8 mm above the bottom. After concreting, the sensor arrays and the cables are completely surrounded and overlaid by screed. Thus, the top surface of the screed is a homogeneous, clean, and closed to minimise the influence of the embedded sensors. Two USB-6210 data acquisition systems from "National Instruments" with a 16-bit resolution are used to record the data from the embedded sensors. All discussed humidities in this study are temperature

compensated. The corresponding measurement data are available online [23].

A high precision balance with a maximum load of 72 kg and an accuracy of 0.1 g is used as reference measurement system. All screed samples are weighed at each measurement day. These gravimetric measurements give a precise and reliable reference of the averaged water content of each sample and holds as reference for the predicted total free liquid water in the pores. The corresponding measurement data are available online [23].

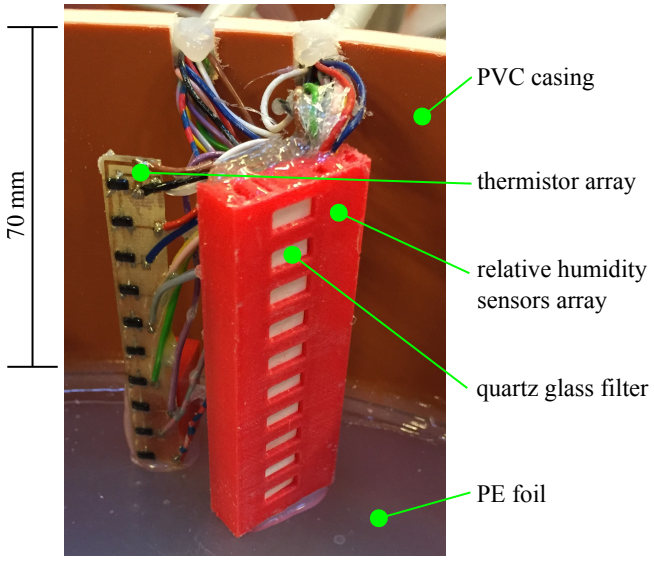

Figure 1: Photograph of embedded sensor arrays (before concreting) which measure relative humidity and temperature at 10 depth position at vertical distances of 6 mm

3.3. Pore size distribution

The discussed mass balance in equation 1 gives a relation between the moisture flux and the pore saturation. Thereby, the exact knowing of the pore distribution ϕ is required. Figure 2 illustrates the cumulative pore volume for three different screed types. These pore distributions are based on a combination of mercury intrusion porosimetry and gas adsorption [24, 25]. The mercury intrusion porosimetry generates test pressures between 0.01 MPa and 400 MPa. The conversion from pressure to a certain pore radius includes the Washburn

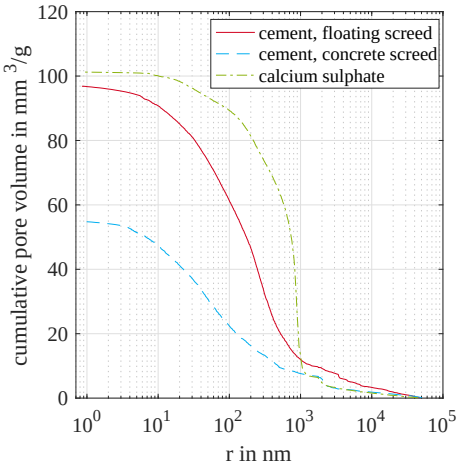

Figure 2: Measured cumulative pore size distribution of three investigated screeds based on gas sorption and mercury intrusion porosimetry

equation [26]. The measurement procedure is the exact reproduction of the international standard [24]. The calculated pore radius starts at approximately 50 μm and sensitivity is recorded to a minimum pore radius of approximately 2 nm. The used dry sample masses are between 0.8 g and 1.5 g and the model assumes cylindrical pores to convert pressure into pore sizes. The other used method is the gas sorption [25, 27] based of the physisorption of nitrogen gas at 77 K in a pressure ranges of 4.5 mbar to 1 bar. The conversion from pressure to a certain pore diameter is based on the BJH theory [28]. The BJH theory includes the layer thickness of the adsorbed nitrogen according to Halsey [29] and the Kelvin equation for calculating the pore radius. The sample mass varies between 1 g and 4.5 g. The measurement procedure is the exact reproduction of the international standard [27]. The measured pore radii are between 0.9 nm and 100 nm. At small pore radii, 0.9 nm to approximately 10 nm, the gas adsorption shows a significantly higher sensitivity as compared to the mercury intrusion. The corresponding measurement data are available online [23].

The two porosimetry measurements are merged together to cover all pore radii. At pore radii at around 5 nm, most pressure steps of the mercury intrusion porosimetry cannot enter further pore volume. Thus, the pore volume of the

associated pore radii becomes zero. This leads to a very wriggly pore size distribution. For these and smaller pore radii, the gas sorption is considered to be more appropriate for our analysis. The point of too "wriggly" mercury intrusion results depends on material and is chosen by eye. For the cement-based floating screed, gas sorption results are used for radii between $0.85 \leq r \leq 5.55$ nm, for the cement-based concrete screed gas sorption is used for radii between $0.9 \leq r \leq 3.55$ nm, and for the calcium-sulphate screed radii between $0.9 \leq r \leq 5.6$ nm. The used gas sorption results in the chosen range consist of approximately 13 sampling points. Then, the mercury intrusion porosimetry with around 400 sampling points is added to a maximum pore radius of 85 μm. Figure 2 represents the cumulative pore distribution for two CT screeds and one CA screed. The calcium-sulphate screed possesses a dominant pore radius of around 1000 nm. The contribution of pore radii less than 10 nm is almost insignificant. The total porosity is around 21%. The cement-based floating screed has a similar total porosity of around 20% whereas no dominate pore radius exists. The pore distribution tends to an uniform distribution over the entire measured range. Furthermore, even the smallest measured pore radii still contribute significantly to the overall porosity. The cement-based concrete screed reveals a pore distribution which tends towards an uniform distribution and the pore volume with small radii remains significant. However, the total porosity is around 12.5%, which leads to a lower total water absorption.

4. Implementation of the theory and data processing

First, this chapter summarises the required parameters to predict the saturation of a pore with a distinct radius. Then follows a discussion of the numerical method which solves the system of transcendental equations. At the end, the processing of the measured values of the embedded sensors is explained.

4.1. Prediction of saturation of a single pore

Table 2 recapitulates the used parameter to compute the pore saturation. All parameters are defined at a standard ambient pressure of $p_0 = 101325$ Pa and an

parameter	numeric value	unit
C	15	
M	0.0180153	kg/mol
R	8.314	J/molK
t_w	0.35	nm
γ	72232	N/m
ρ_l	0.99754	kg/m^3

Table 2: Material parameters and properties used for free liquid water and water vapour at 296 K

ambient temperature of $T = 296$ K. Equation 3 and 4 determine the adsorbed water layer t_w. Mathematically, two solutions exist, although only the solution for the smaller t_a is valid. However, this system of transcendental equations does not have an analytical solution. For $h \to h_m$, the two solutions are located close to each other, thus a classical Newton's method in optimisation becomes unstable. Therefore, a fixed-point iteration of $t = t_a(h, h_m(t, r)) =: g_{h,r}(t)$ is used. The function g is contractive, thus all iterations converge towards the solution. The initial layer thickness is 0.001 nm and the required accuracy to interrupt the iteration is 10^{-6}.

Figure 3 reveals the computed pore saturation based on the approach of Hillerborg [13] for the parameters shown in table 2. For cylindrical pores with pore radii between $r = 1$ nm and 2000 nm, the pore saturation s as a function of the humidity is illustrated. On top of the plot, the corresponding maximum humidity h_m is depicted. For example, for a common ambient relative humidity of 50%, pores with $r = 1$ or 2 nm are already completely saturated. A pore with $r = 10$ nm is $s = 13.5\%$ water-filled and for $r = 200$ nm, the saturation is around $s = 0.66\%$. For $h > 0.95$ rH, the increase of pore saturation is highly exponential, especially for larger pores. Thus, for high humidity, the measurement uncertainty becomes higher.

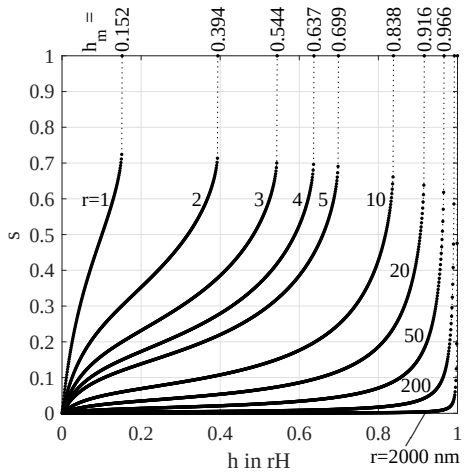

Figure 3: Pore saturation of a single pore depending on the ambient relative humidity h based on the approach by Hillerborg; all pore radii are given in nm

4.2. Data processing of embedded humidity sensor arrays

One embedded array for thick samples consists of 10 relative humidity sensors. The topmost sensor has a distance of around 8 mm to the top surface of the screed sample. To analyse the entire sample, this gap is linearly interpolated. Thus, a relative humidity of $h = 50\%$ rH is assumed directly at the top surface of the sample. This value is identical to the ambient relative humidity in the climate chamber and thus, incorporates the required continuity of thermodynamic quantities. The bottommost sensor has a distance of around 8 mm to the bottom. To capture this gap, the relative humidity measured by the bottommost sensor is assumed to remain constant down to the sample bottom. Thus, 10 measured humidities and two boundary conditions exist. To obtain the desired resolution of 0.1 mm, the humidity is interpolated linearly over the entire sample. This simple and ordinary approach of fitting the humidity data does not incorporate the high non-linear behaviour of convective and diffusive moisture transport. Nevertheless, this approach is used because of its high robustness. Non-linear interpolation, i.e. cubic splines, or extrapolation from the sensor position to the top surface or the bottom may give non-physical trends

and values. For the sake of robustness, linear interpolation and constant extrapolation to the bottom is chosen.

Furthermore, all measured humidities have to be below 95% to be used for the absorbed water prediction. We assume that the measured pore volume distribution is representative for the entire sample and that the moisture transport is symmetric to the surface normal. Hence, for every 0.1 mm step of the sample, the pore saturation is computed and the free liquid water is calculated based on the pore distribution. A summation over the sample hight yields the total adsorbed water based on the dry weight of the sample. The sample weight including embedded sensors is measured before concreting and always subtracted. Thus, the screed net weight is known. Cement based-samples are drying at 378 K and calcium-sulphate-based samples are dried at 313 K and an ambient relative humidity of less than 10% rH is maintained until a constant weight is reached.

5. Results and Discussion

First, the distribution of the humidity inside the screed samples is shown based on the embedded sensors. Then, the theory is validated via the measured sample weight. Based on this satisfying validation, the spatial and temporal distribution of the absolute water content is presented. A separation of capillary and inkbottle water during desorption follows. Finally, an approach to predict the sorption isotherm is discussed.

5.1. Spatial and temporal distribution of the corresponding relative humidity

Figure 4 shows the distribution of the relative humidity for a thick calcium-sulphate screed sample over time. This contour plot represents the interpolated relative humidity based on 42 measurements. At the beginning, the embedded humidity sensors reach saturation in the fresh screed. On day 12, the topmost sensor leaves saturation. From then on, sensors start to leave saturation from top to bottom. A clear dehydration gradient is visible due to screed hydration

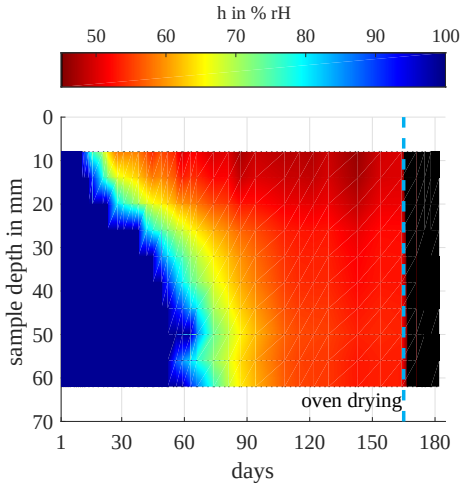

Figure 4: Spatial and temporal distribution of the corresponding relative humidity for the calcium-sulphate screed with 70 mm sample thickness presented as a two-dimensional contour plot [23]

and evaporation. On day 66, all sensors leave saturation. The topmost sensor with $h = 51\%$ rH almost reaches the equilibrium moisture content of 50% rH predefined by the climate chamber humidity. On day 164, the last measurement in the climate chamber reveals a maximum of $h = 53\%$ rH in the sample. At this point, the sample is considered to have reached the equilibrium moisture content completely. A period of 18 days of oven drying follows to determine the dry screed net weight and the corresponding moisture content in percent by weight [10].

5.2. Comparison of the predicted water loss and the measured balance weight

Based on the embedded humidity sensors, the pore saturation is computed and the moisture transport predicted. If water evaporates, the screed sample becomes lighter and the humidity is decreasing. As mentioned before, the sample weight is measured by a high precision balance. Hence, global moisture variations are monitored and quantified in g. For comparison, the adaption of Hillerborg's theory and its integration over the entire sample yields the variation of moisture in g as well. A direct comparison of the measured weight and the

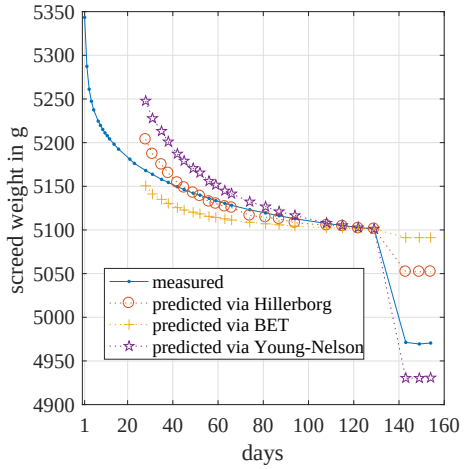

Figure 5: Predicted sample weight and measured balance weight for cement-based floating screed with 35 mm sample thickness

predicted weight loss serves as validation. Figure 5 depicts the decrease of the total sample weight over time for the thin cement-based floating screed sample [23]. On the first day, the total net screed weight is 5343 g and at the end 4971 g after oven drying. On day 28, all five humidity sensors leave saturation which allows the computation of the total absorbed water. The last weight measured before oven drying is used to correct the bias of the screed weight. Between day 42 and day 129, the measured screed weight decreases by 49 g. In this period, the maximum deviation between the measured weight and the predicted water loss is 6 g. Thus, the two approaches reveal a satisfying correlation. For comparison, the classical Brunauer-Emmett-Teller (BET) theory and the Young-Nelson theory are applied to this pore system as well. The classical BET theory assumes only flat surfaces, thus the pores have a slit shape instead of a cylinder shape. Thus, the surface tension remains constant for all pore radii and saturation levels [13, 14]. Figure 5 yields that the BET theory underestimates the total water loss significantly during evaporation and oven drying. As already discussed, the BET theory assumes only slit shaped pore. Thus, the theory does not consider the variation of the vapour pressure due to the curved liquid-vapour interface at the inner layer. Hence, the slit shaped pores leave saturation much early

compared to cylinder shaped pores [13]. Thus, the BET theory is unable to quantify correctly the moisture in pores at higher humidities, including multi-
355 layers of adsorbed water. The Young-Nelson theory does not consider the pore size distribution at all. The theory predicts the unimolecular bound moisture and the normally condensed moisture based on the density of considered material as well as the density water [30]. According to the other two theories, the parameter accounting for the heat of adsorption of the molecules bound to the
360 surface is set to $E = 0.0667$. The assumed monolayer moisture content for a 90 days old screed is $v_m = 0.045$ [31]. Figure 5 shows that the Young-Nelson theory significantly overestimates the water release during evaporating as well as oven drying. Following Young-Nelson's theory, an infinite number of molecular layers of water can be stacked on top of the material surface. This assumption might
365 hold for macroscopic materials like corn, for which the theory was originally intended. Nevertheless, in building materials, microscopic pores with diameters of few nm exist. If a pore is already fully saturated, a further increase of the water vapour partial pressure does not increase the moisture. On the contrary, the Young-Nelson theory would lead to a further, and thus non-physical, in-
370 crease in material moisture. This inability of the theory to account for the pore geometries cause the significant overestimation of the water release in screed during evaporation and oven drying.

Figure 6 depicts another cement-based screed sample. The used material is cement-based concrete screed. As discussed above, the total porosity of 12% is
375 significantly lower compared to the other two screed types. Thus, the water loss per unit volume is expected to be lower. The initial weight of this thick sample is around 10100 g and the first measurement with all humidity sensors out of saturation is performed after 122 days. After 437 days, almost the entire sample reachs the equilibrium moisture content of $h = 50\%$ rH. At lower moisture levels,
380 approximately below $h = 80\%$ rH, the capillary convection tends towards zero and the evaporation process is dominated by diffusion. With a screed sample thickness of 70 mm, the diffusion process takes much more time compared to thin samples with a thickness of 35 mm. Besides the first measurement point,

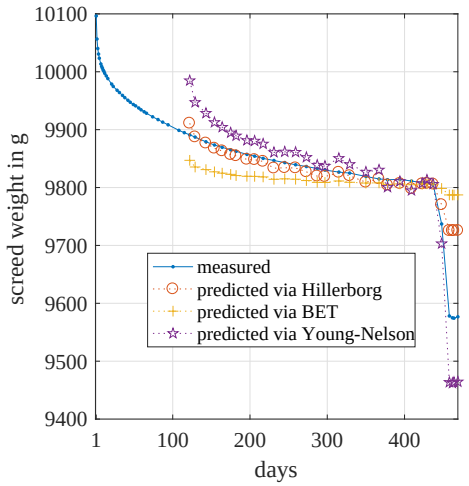

Figure 6: Predicted sample weight and measured balance weight for cement-based concrete screed with 70 mm sample thickness

the highest deviation is observed at day 231 with a difference of 14 g. Although the predicted water release shows some scatter, the total water loss of 81 g water during day 129 and day 437 is reproduced correctly. According to the cement-based screed discussed above, the theory and the measured weights after oven drying deviate significantly.

Furthermore, the two other theories show a similar behaviour compared to the other cement-based screed. Again, the BET theory underestimates the water release and the Young-Nelson theory overestimates the water release. Based on the two considered cement-based screeds, Hillerborg's theory seems to be the most accurate theory for porous building materials including such fine pore structures. Figure 7 illustrates the thick calcium-sulphate screed sample. In contrast to the two previous samples, this is a calcium-sulphate-based screed. The diffusivity material constant for cement based materials is assumed to be $C = 15$ [31]. The same diffusivity is assumed for calcium-sulphate-based materials. C depends on the ambient temperature and the net heat of adsorption of the corresponding material. At room temperature, these values remain almost constant. The same constant $C = 15$ is used for calcium-sulphate-based screeds.

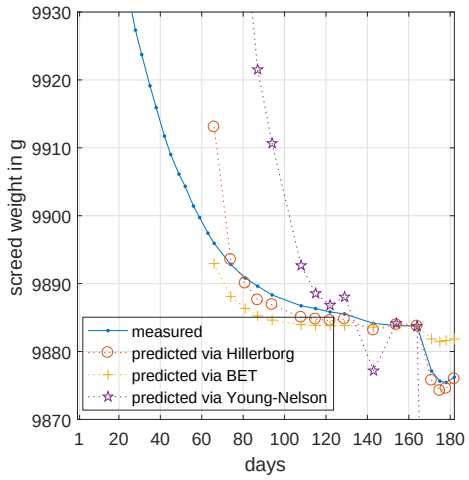

Figure 7: Predicted sample weight and measured balance weight for the calcium-sulphate screed with 70 mm sample thickness

On the first day, the sample weight is 10655 g, which decreases to 9884 g before oven drying and to 9876 g afterwards. Beside the first measurement point, the agreement between the predicted water loss and the measured screed weight is satisfying for calcium-sulphate-based screeds as well.

Furthermore, the water loss during the oven drying is predicted correctly by the theory. In the case of the two cement-based samples, the real water loss is significantly higher compared to the predicted one. One reason is the different oven drying process. The calcium-sulphate screeds are dried at 313 K, the cement based screeds are dried at 378 K. The temperature is significantly higher and hence, the thermal activity of the water increases. At 378 K, besides evaporation of free liquid water, bound water molecules in the calcium-silicate-hydrate (C-S-H) phase may leave the cement matrix and the screed weight decreases. The relative humidity sensors are not able to recognise this process. Chemically bound water in the C-S-H phase does not influence the thermodynamic equilibrium between the free liquid water and the corresponding relative humidity in the pores. Changes of the amount of bound water leads always to a systematic deviation. At 313 K drying temperature, bound water molecules probably do

not leave the calcium-sulphate matrix and the oven drying decreases the amount of free liquid water only. This evaporation directly affects the thermodynamic equilibrium and is recognised by the relative humidity sensors. Thus, the weight loss of 8 g water during the oven drying is correctly predicted by the presented theory.

The two other theories are included as well in figure 7. The classical BET theory underestimates the water release. Nevertheless, the BET theory is quite close to the Hillerborg theory and the measured values during evaporation. As shown in figure 2, this calcium-sulphate screed posses an almost unimodal peak pore at approximately $r = 1000$ nm. The pore volume of smaller pore ($r < 10$ nm) is comparably low. For pores with $r = 1000$ nm, the differences of pore saturation between an assumed cylinder shape or slit shape become low because the increase of surface tension due to curved liquid-vapour interface at the inner layer becomes low as well. Based on observations in figure 7, this claim can be made: the bigger the pores in porous materials, the closer the BET theory is to measured values. Nevertheless, the BET theory fails again to estimate the water release correctly during oven drying. The relative humidity in the oven is close to zero and small pores become empty or partially saturated as well. At such low humidities, the curved liquid-vapour interface at the inner layer has a high influence although their total pore volume is small. This gives rise to the deviation between the BET and the Hillerborg theory. The Young-Nelson theory completely fails for the considered calcium-sulphate screed. The water release is highly overestimated and the predicted line in figure 7 exceeds the range of the plot. From this theory, one would expect a better agreement between the Young-Nelson theory and the measurements. The unimodal peak pore with $r = 1000$ nm is comparably big and high number of water layers may be stacked before the pore becomes fully saturated. Thus, the authors believe that the assumed monolayer moisture content of $v_m = 0.045$ (adapted to cement-based materials) is inappropriate for calcium-sulphate materials. The correct v_m for calcium-sulphate based materials remains questionable.

A comparison of all three discussed screed types in figures 5 to 7 and all three

theories, Hillerborg's theory shows the best agreement. The correlation of measured weight loss and theoretically predicted water release is significant. Hence, the proposed adaption of Hillerborg's theory for a complete pore volume distribution is considered well supported by this study.

5.3. Free liquid water distribution in wt.%

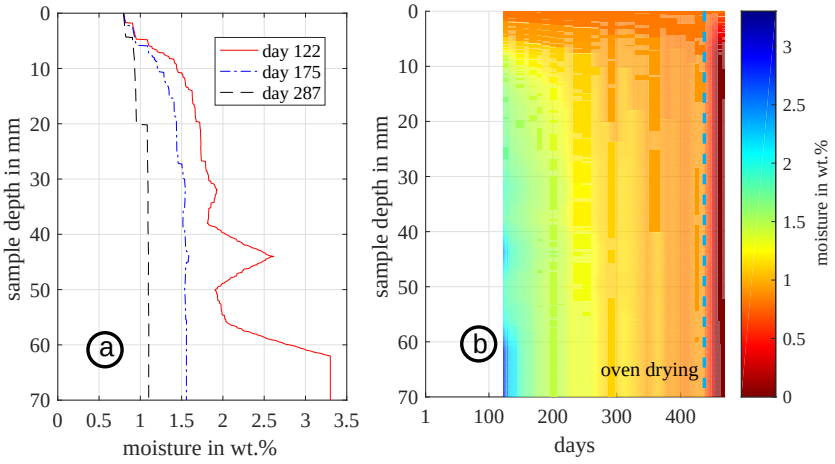

Figure 8: Spatial and temporal free liquid water distribution in wt.% for cement-based concrete screed with 70 mm sample thickness; a: free liquid water distribution of day 122, 175, and 287; b: presentation as a two-dimensional contour plot

Based on the satisfying validation of the predicted adsorbed water for the entire screed sample, the moisture in percent by weight is calculated at every of 701 sampling points leading to a spatial resolution of 0.1 mm. Figure 8 illustrates the moisture results over time and sample thickness of 70 mm. In figure 8 a, the moisture over the sample thickness is presented for three distinct days. In figure 8 b, the same data for all measurement days are illustrated as a two-dimensional interpolated contour plot. The solid line in figure 8 a corresponds to the first data line in the contour plot in figure 8 b. At day 122, all sensors leave saturation and the moisture is predicted for the entire sample. At 8 mm depth (topmost sensor position), the moisture is at 1.35 wt.%. It increases towards the bottom and reaches a maximum of 3.3 wt.%. At 44 mm depth, there

is a local area with high moisture. It is expected that the moisture continuously increases toward the bottom because evaporation occurs only on the top surface. Thus, this local peak at 44 mm depth is expected to be measurement deviation of the humidity sensor. At this high humidity level, small deviations have a high influence on the calculated saturation. On day 175, the moisture gradients inside the sample are reduced significantly. The moisture increases from 0.79 wt.% at the top surface to approximately 1.5 wt.% at 20 mm depth. At a higher depth, the moisture content remains almost constant toward the sample bottom. At day 287, the moisture increases only slightly toward the bottom. The homogeneous moisture distribution indicates that the sample has almost reached its equilibrium moisture content. Nevertheless, it takes more than 380 days in total until the sample indeed features the equilibrium moisture content of around $h = 50\%$ rH. On day 437, the moisture is constant in the cross section and the mean moisture amounts to 0.91 wt.%. Between day 122 and day 200, the moisture changes in the upper 20 mm of the sample are low. On the contrary, the areas below 30 mm depth with moisture of around 2 to 3.3 wt.% disappears much faster. On day 154, the maximum moisture is 1.73 wt.%. In fact, a moisture decrease from around 3.3 wt.% to 1.73 wt.% takes 32 days, an additional decrease from 1.73 wt.% to 0.91 wt.% takes 283 days. This indicates a transition from a capillary convective process to a diffusion dominated moisture transport. Although the upper third of the sample remains almost unaffected between day 122 and 154, which indicates that the moisture transport to the sample surface is highly dominated by diffusion, a capillary convective moisture transport in the lower third still takes place. Thus, the water inside this "insular moisture area" in the lower third has a much higher mobility in the porous system. Consequently, the moisture transport models have to take into account this transition from convection to diffusion inside the sample. Hence, globally defined material constants like diffusivity and conductivity are not sufficient for samples outside a global thermodynamic equilibrium including high moisture gradients. After oven drying, the measured humidity is at around $h = 8\%$ rH, which corresponds to ca. 0.02 wt.% moisture.

The spacing of the embedded humidity sensor array and the adaption of Hillerborg's approach for a continuously given pore volume distribution reveals the absolute free liquid water content or, by knowing the dry screed weight, the local moisture in wt.% inside the sample with a high spatial resolution. This yields a much deeper insight into moisture transport and associated processes like thermal and hygric expansion, penetration and mobility of chlorides and other substances, formation of diffusion barriers during the alkali-silica reaction, etc.

5.4. Separation of capillary and inkbottle water

As discussed in equation 7, the total pore saturation S_{total} consists of two terms. S_{cp} represents the capillary water in the pores. It is based on the assumption of a thermodynamic equilibrium between the free liquid water and the water vapour. This equilibrium is identical for the adsorption and desorption process. In the case of desorption, the inkbottle effect S_{ink} contributes to the total pore saturation as well. If a large pore is connected to the pore system by only smaller pores, the larger pore remains fully saturated until the smaller connecting pore leaves saturation. The probability of a trapped pore is f. However, the embedded humidity sensor arrays enable the separation of these two effects. Figure 9 depicts the total water in the sample made of cement-based floating screed. This line is identical to figure 5. The two other lines represent the capillary and the inkbottle water. The summation of both terms yields the total water according to equation 7. At day 28, the capillary water amounts to 58.05 g and the inkbottle water to 98.05 g. Thus, 62.81% of the total water is trapped in larger pores. This ratio remains almost constant, for example, 64.34% on day 66 and 62.63% on day 129. After oven drying, the two terms are similar whereas the capillary water is slightly higher compared to the inkbottle water.

Figure 10 illustrates the same separation for the calcium-sulphate screed. At day 66, the total water amounts to 50.18 g and the inkbottle water to 30.19 g. Hence, 60% of the total water are enclosed in larger pores. At day 74, the inkbottle water with 16.31 g is only slightly higher than the capillary water

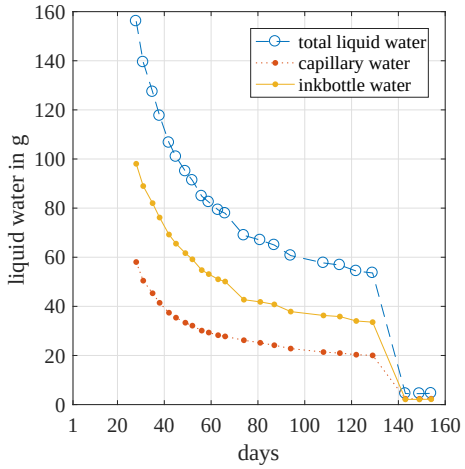

Figure 9: Separation of capillary and inkbottle water for the cement-based floating screed with 35 mm sample thickness

with 14.36 g. Hence, only 53.2% of the water is trapped in larger pores. This ratio decreases slightly to 51.94% at day 164. The different behaviour of these two samples is a direct outcome of the pore volume distribution shown in figure 2. The total porosity of materials is almost similar with around 21%. Nevertheless, the pore distribution is different. In the case of the cement-based floating screed, the pore volume is uniformly distributed over a wide pore size of 1 nm$< r <$ 100 μm with a slight accumulation at $r \approx 500$ nm. Based on this uniform distribution, the probability of trapped water remains constant as well. In contrast, the calcium-sulphate screed possesses a unimodal pore size distribution at $r \approx 1000$ nm. The pores smaller than $r < 100$ nm and larger than $r > 2000$ nm contributes only with a small share to the total pore volume. Thus, the inkbottle water is influenced by this dominant pore size as well. The dryer the screed becomes, the lower the probability of water enclosed in pores close to the radius of the dominant pore. The inkbottle water is influenced by distance of the critical pore radius and the dominant pore. Consequently, the percentage of inkbottle water decreases. Although the pore size distribution shows a dominant pore size, the inkbottle water still exceeds the capillary water. Furthermore, the larger the influence of inkbottle water, the higher the

hysteresis of the isotherm between adsorption and desorption.

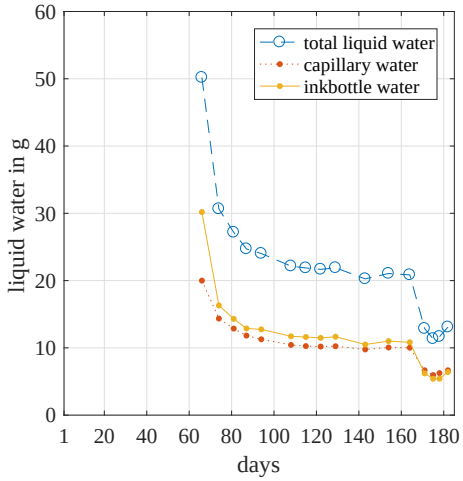

Figure 10: Separation of capillary and inkbottle water for the calcium-sulphate screed with 70 mm sample thickness

5.5. Sorption isotherm hysteresis

The hysteresis between adsorption and desorption is mainly caused by trapped water in the pore system. This effect is described by the inkbottle water in the presented theory. Following this interpretation, hysteresis is directly derived from the pore geometry. Given a pore volume distribution and assuming geometrical connection between pores of different sizes, the adsorption and desorption isotherm is known for any ambient humidity. In figure 11, the sorption isotherms for the cement-based floating screed and the calcium-sulphate screed are shown. As mentioned before, the pore volume distribution is based on mercury intrusion porosimetry and gas sorption and the assumption of a random pore distribution. Hence, the entire sorption isotherm is determined for $0\% \leq h \leq 100\%$. These isotherms must be regarded as qualitative data because no experiments of validation for our screed samples exist so far. Nevertheless, the general trend is consistent. The cement-based screed yields higher moisture levels in wt.% for a given humidty as the calcium-sulphate screed although both screeds possess a similar porosity of around 21%. In the presented case,

the limits for ready for flooring of 0.5% (CA) and 3.5% (CT) are reached at around 88% rH and 79% rH, respectively. Furthermore, the amplitude of the hyseresis for the cement-based screed is significantly higher. At $h \leq 11.3\%$ rH, adsorption and desorption are identical for both screeds because the smallest measured pore with $r = 0.85$ nm leaves saturation. At this point, there is no completely filled pore that may entrap water in larger pores.

Reducing the sorption hysteresis only on the geometry of the pore system is a strong simplification, especially under the assumption of a constant diffusivity. However, this approach only requires the pore volume distribution which is measured within hours. Experimental determination of the sorption isotherm with reference specimens in climate chamber takes several months. This quick approach gives a good qualitative estimation of the sorption isotherm and its hysteresis.

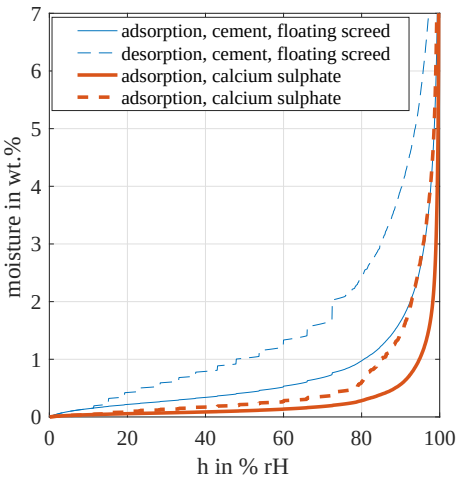

Figure 11: Predicted sorption isotherm for cement-based floating screed and the calcium-sulphate screed at an ambient temperature of 296 K

5.6. Error discussion

Humidity sensor arrays are embedded in 16 samples with 8 different screed types. For 7 screeds, the correlation between the measured balance weight

and the predicted water release is shown to be conclusive. Only the cement-based rapid screed shows systematic deviations (whereas the cement-based rapid heated screed shows good agreement). For this sample, the mercury intrusion porosimetry shows an odd behaviour. Pores smaller than $r = 12$ nm do not exist, probably caused by an inaccurate porosimetry measurement. Nevertheless, 14 of 16 samples show a high correlation and the proposed experimental and theoretical approach is considered to be conclusively supported by our data. Nevertheless, small deviations and data scatter exist for all samples. The main factors affecting the accuracy are discussed in the following.

The sampling from the mercury intrusion porosimetry and gas adsorption was taken after a drying period of approximately six months. Although the hydration of the cement matrix of the screeds samples will never end, the rate reduces during hardening. After six months, the pore system is supposed to be stable and the hydration process may be neglected. On the other hand, carbonation may close smaller pores, the smaller pores are crucial for the inkbottle effect. In our experiment, no measurements exist to quantify this effect. Nevertheless, the six month period of drying and hardening is expected to result in a good balance between variations of the pore system due to hydration and carbonation.

During the comparison between theory and measured sample weight, the predicted water amount is overestimated for all three screed types shown during the first measurement days. Three main reasons are identified to cause the systematic deviation. The first one is the pore saturation process itself. In figure 3, the pore saturation is illustrated. At high humidities, the saturation increases highly exponentially. For example, a pore with a radius of $r = 200$ nm at $h = 98.2\%$ rH is saturated by $s = 21.88\%$. At $h = 99.2\%$ rH, the pore is already completely filled. For larger pores, the exponential growing of saturation is even higher. Furthermore, at high humidities above $h = 90\%$ rH, the humidity sensor accuracy amounts to $\pm 7\%$. Therefore, at high humidities, these two effects intensify the uncertainty of the measurement accuracy significantly. To counteract this effect, measured humidities only below $h = 95\%$ rH are considered for further computation. Still at this humidity threshold, small measurement variations of

the humidity lead to large deviations. The second reason is the negligence of the source/sink term Q in equation 1. The prediction of the free liquid water is based on the assumption of a thermodynamic equilibrium between the free liquid water and the water vapour. If free liquid water disappears, the humidity decreases and a weight loss is computed. Nevertheless, the free liquid water may evaporate or become chemically bound in the cement matrix. In the latter case, the weight of the sample does not change although the free liquid water is reduced. Thus, the negligence of the sink term Q always leads to an overprediction of the weight loss as long as hydration in the cement matrix occurs. Pane et al. quantifies the hydration for ordinary Portland cement in experiment [32], Di Luzio et al. in simulations [33]. At 296 K, most hydration takes place during the first 28 days. Nevertheless, after 166 days, the hydration is still ongoing at a low rate. This is consistent with our measurements. The cement-based floating screed in figure 5 shows a systematic overprediction of the weight loss between day 28 and day 45 indicating that hydration is still active. The two other samples including first free liquid water predictions after 66 and 122 days have an overprediction only for the first measurement point (which is probably related to the first discussed reason of deviation). The third reason is a direct consequence of the hydration process. Hydration leads to the formation of the porous cement matrix. Hence, the evolution of the pore system is an ongoing process. The determination of the pore volume via mercury intrusion porosimetry and gas adsorption is performed 6 months after concreting. Hence, the used pore volume distribution may not be representative until the hydration is finished.

In addition, the drying of the screed samples in the oven itself may also cause differences between the predicted and the measured water loss. Åhs [34] shows that the first drying cycle at $h \ll 10\%$ rH alters irreversibly the C-S-H phase. So called "gentle drying" at $h = 10\%$ rH reduces the alternation of the C-S-H phase because less interlayer water is removed. Nevertheless, these water molecules in the C-S-H phase do not contribute to the thermodynamic equilibrium between the free liquid water in the pores and the water vapour. Thus the discussed approach cannot account for these variations in the C-S-H phase.

In general, aggregates do not contribute to the pore system or the moisture transport. The size, amount, and material of aggregates for the 8 different screeds are unknown. Thus, the dry weight of the screeds is assumed to consist completely of cement without aggregates. Although for the used screed types, this assumption seems to be correct, for concrete with large aggregates, the grading curve has to be known. The negligence of aggregates may cause a systematic deviation between the measured sample weight and the predicted water loss.

A further uncertainty is the used moisture diffusivity constant of $C = 15$ according to [13, 15, 16]. Our experiments are performed in a climate chamber at constant ambient temperature of 296 K and the entire process is treated as isothermal. Under isothermal condition, the diffusivity of Portland cement varies between $10 < C < 50$ [31]. Using a suggested approximation leads to a diffusivity of $C = \exp(\frac{855}{T}) = 17.96$ [19, 31]. Furthermore, the constant C greatly increases as the cement matrix is oversaturated [35]. This observation may explain the fast decay of areas with moisture of more than 3 wt.% in figure 8. Consequently, this means the assumption of one constant diffusivity is questionable if high moisture gradients exist. Moreover, all cited publications regarding the diffusivity only consider Portland cement. In our experiments, the four cement-based and four calcium-sulphate-based screeds are used. No details about the chemical composition of the cement including additives and aggregates are known. Therefore, choosing the right C for arbitrary screeds is still an open question which cannot be answered by our experiments.

Further uncertainty is generated by the description of the pore system. Transforming the partial pressure of the Kelvin equation into a pore size requires a geometric model. Cylindrical pores are assumed, but in reality, pores have all kinds of geometry, shape, and turtuosity. Furthermore, the computation of the inkbottle water assumes a totally random distribution. Nevertheless, certain pore-connections may be privileged and this would influence the inkbottle effect significantly.

6. Conclusion

In this study, we investigated eight different types of screed during hydration and evaporation to monitor moisture transport. For this purpose, 10 humidity sensors were successfully embedded in every screed sample. The sensors themselves were protected by filter membranes. The hydration process was monitored for months until the equilibrium moisture content is reached. The sensors had a high sensitivity at moderate and low moisture content. All moisture changes were continuously monitored via the measurement of the relative humidity.

For several applications in civil engineering, the knowledge of the absolute moisture content is of much higher interest than data of the relative humidity in the pore system. The functional relation between these two quantities is the adsorption isotherm. Unfortunately, the exact function is unknown for almost all building materials. To close this lack of knowledge, we adapted the theory by Hillerborg to calculate the pore saturation. With this approach and the known pore volume distribution, we predict the absolute water content in porous materials without usage of the sorption isotherm. By knowing the dry weight of the screed, we are also able to convert the humidity into moisture in percent by weight.

By this theoretical approach, the hydration and evaporation of different screed samples are predicted accurately. The good agreement between the computed water loss based on the embedded humidity sensors and the sample weight decrease measured by a high precision balance is conclusive. Hence, this new approach of experimental measurements of the free liquid water content in porous materials is considered as validated for the investigated screed types and the chosen ambient conditions. This approach enables the non-destructive, calibration-free evaluation of the moisture in percent by weight with a high spatial resolution in the order of mm over long periods of time such as months or years. The proposed approach may be adapted to several investigations regarding moisture transport. Embedded sensors enable a robust monitoring of hazardous moisture in crucial components of infrastructure and building con-

struction.

In case of desorption, the amount of capillary and "entrapped" inkbottle water are predicted separately. It is shown that the pore volume distribution directly affects the amount of inkbottle water and the shape of the desorption isotherm. The computation of the inkbottle effect gives a first attempt to predict the hysteresis of the sorption isotherm for humidity ranging from 0% to 100% rH.

Passive humidity sensors may be embedded into concrete directly during the construction [36]. Based on such an approach, the humidity is measured for several years or decades. This would monitor the temporal variation of the humidity due to varying ambient conditions, loads, or material degradation.

Our approach enables a non-destructive, calibration-free moisture monitoring. The sensors possess high capability to detect moisture-induced deteriorations at early stage and prevent costly repair works months or years later. This makes infrastructure and building construction much safer, more cost-efficient, and highly reliable.

7. Acknowledgement

The authors are grateful to Felix Hase for setting up the embedded sensors, to Sarah Nagel for taking several measurements of the screeds over months, to Carsten Prinz (BAM, 1.3) for measuring the pore volume distribution, and to Dr. Stefan Born (TU Berlin) for helping with the fixed-point iteration approach.

References

[1] U. Nürnberger, Korrosion und Korrosionsschutz im Bauwesen. Band 1 und 2, Bauverlag Wiesbaden/Berlin, 1995.

[2] S. Kruschwitz, Assessment of the complex resistivity behavior of salt affected building materials, Ph.D. thesis, Technische Universität Berlin (2007).

[3] F. Weise, K. Voland, S. Pirskawetz, D. Meinel, Analyse akr-induzierter schädigungsprozesse in beton, Beton-und Stahlbetonbau 107 (12) (2012) 805–815. doi:10.1002/best.201200049.

[4] K. Kupfer, Materialfeuchtemessung: Grundlagen, Meßverfahren, Applikationen, Normen, Expert-Verlag, 1997.

[5] R. Černỳ, Time-domain reflectometry method and its application for measuring moisture content in porous materials: A review, Measurement 42 (3) (2009) 329–336. doi:10.1016/j.measurement.2008.08.011.

[6] ASTM International, Standard test method for determing relative humidity in concrete floor slabs using in situ probes, F2170-16b.

[7] L. J. Parrott, Moisture profiles in drying concrete, Advances in Cement Research 1 (3) (1988) 164–170. doi:10.1680/1988.1.3.164.

[8] M. Vinkler, J. L. Vítek, Drying concrete: Experimental and numerical modeling, Journal of Materials in Civil Engineering 28 (9) (2016) 1–8. doi:10.1061/(ASCE)MT.1943-5533.0001577.

[9] Technische Kommission Bauklebstoffe, TKB-Bericht 2: Belegereife und Feuchte Die KRL-Methode zur Bestimmung der Feuchte in Estrichen, Merkblatt TKB-B 2, Industrieverband Klebstoffe e. V. (Juli 2013).

[10] C. Strangfeld, S. Kruschwitz, J. Wöstmann, S. Nagel, F. Hase, Moisture in screed: a non-destructive multi-sensor approach, in: 8th European Workshop on Structural Health Monitoring, Bilbao, Spain, 2016, pp. 1–11.

[11] R. M. Espinosa, L. Franke, Influence of the age and drying process on pore structure and sorption isotherms of hardened cement paste, Cement and concrete research 36 (10) (2006) 1969–1984. doi:10.1016/j.cemconres.2006.06.010.

[12] A. Kumar, S. Ketel, K. Vance, T. Oey, N. Neithalath, G. Sant, Water vapor sorption in cementitious materials-measurement, modeling and

interpretation, Transport in Porous Media 103 (1) (2014) 69–98. doi:10.1007/s11242-014-0288-5.

[13] A. Hillerborg, A modified absorption theory, Cement and Concrete Research 15 (5) (1985) 809–816. doi:10.1016/0008-8846(85)90147-4.

[14] S. Brunauer, P. H. Emmett, E. Teller, Adsorption of gases in multimolecular layers, Journal of the American Chemical Society 60 (2) (1938) 309–319. doi:10.1021/ja01269a023.

[15] R. P. Chaube, A study of the moisture transport process in concrete as a composite material, Proceedings of the JCI 16 (1) (1994) 895–900.

[16] T. Ishida, K. Maekawa, T. Kishi, Enhanced modeling of moisture equilibrium and transport in cementitious materials under arbitrary temperature and relative humidity history, Cement and Concrete Research 37 (4) (2007) 565–578. doi:10.1016/j.cemconres.2006.11.015.

[17] DIN, ISO 12571:2013: Wärme- und feuchtetechnisches Verhalten von Baustoffen und Bauprodukten - Bestimmung der hygroskopischen Sorptionseigenschaften, Deutsche Norm, German Standard.

[18] Y. Luan, T. Ishida, Enhanced shrinkage model based on early age hydration and moisture status in pore structure, Journal of Advanced Concrete Technology 11 (12) (2013) 360–373. doi:10.3151/jact.11.360.

[19] W. Zhang, F. Tong, X. Gu, Y. Xi, Study on moisture transport in concrete in atmospheric environment, Computers and Concrete 16 (5) (2015) 775–793. doi:10.12989/cac.2015.16.5.000.

[20] W. Thomson, LX. On the equilibrium of vapour at a curved surface of liquid, The London, Edinburgh, and Dublin Philosophical Magazine and Journal of Science 42 (282) (1871) 448–452. doi:10.1080/14786447108640606.

[21] T. Ishida, R. P. Chaube, T. Kishi, K. Maekawa, Modeling of pore water content in concrete under generic drying wetting conditions, in: Proceedings-Japan Society of Civil Engineers, 1997, pp. 199–210.

[22] F. Hase, Design und Aufbau verschiedener Messysteme zur Ermittlung des Feuchtigkeitsprofiles von Estrich, Bachelor thesis, Hochschule für Technik und Wirtschaft Berlin (2016).

[23] C. Strangfeld, C. Prinz, F. Hase, S. Kruschwitz, Humidity data of embedded sensors, sample weights, and measured pore volume distribution for eight screed types, Construction and Building Materials: Data in Brief (2018) 1–3doi:10.4121/uuid:d2ba436f-78c0-4105-8a1f-5422fcb37851.

[24] ISO, 15901-1:2016(E): Evaluation of pore size distribution and porosity of solid materials by mercury porosimetry and gas adsorption - Part1: Mercury porosimetry, International Standard.

[25] DIN, 66134 : 1998-02: Bestimmung der Porengrößenverteilung und der spezifischen Oberfläche mesoporöser Feststoffe durch Stickstoffsorption, Deutsche Norm, German Standard.

[26] E. W. Washburn, The dynamics of capillary flow, Physical review 17 (3) (1921) 273–283. doi:10.1103/PhysRev.17.273.

[27] ISO, ISO 15901-2:2006(E): Pore size distribution and porosity of solid materials by mercury porosimetry and gas adsorption - Part 2: Analysis of mesopores and macropores by gas adsorption, International Standard.

[28] E. P. Barrett, L. G. Joyner, P. P. Halenda, The determination of pore volume and area distributions in porous substances. i. computations from nitrogen isotherms, Journal of the American Chemical Society 73 (1) (1951) 373–380. doi:10.1021/ja01145a126.

[29] G. Halsey, Physical adsorption on non-uniform surfaces, The Journal of Chemical Physics 16 (10) (1948) 931–937. doi:10.1063/1.1746689.

[30] J. H. Young, G. Nelson, Theory of hysteresis between sorption and desorption isotherms in biological materials, Transactions of the American

Society of Agricultural and Biological Engineers 10 (1967) 260–263. doi:10.13031/2013.39649.

[31] Y. Xi, Z. P. Bažant, H. M. Jennings, Moisture diffusion in cementitious materials - adsorption isotherms, Advanced Cement Based Materials 1 (6) (1994) 248–257. doi:10.1016/1065-7355(94)90033-7.

[32] I. Pane, W. Hansen, Investigation of blended cement hydration by isothermal calorimetry and thermal analysis, Cement and Concrete Research 35 (6) (2005) 1155–1164. doi:10.1016/j.cemconres.2004.10.027.

[33] G. Di Luzio, G. Cusatis, Hygro-thermo-chemical modeling of high-performance concrete. II: Numerical implementation, calibration, and validation, Cement and Concrete Composites 31 (5) (2009) 309–324. doi:10.1016/j.cemconcomp.2009.02.016.

[34] M. S. Åhs, Sorption scanning curves for hardened cementitious materials, Construction and Building Materials 22 (11) (2008) 2228–2234. doi:10.1016/j.conbuildmat.2007.08.009.

[35] Z. P. Bažant, R. L'Hermite, Mathematical modeling of creep and shrinkage of concrete, Wiley New York, 1988. doi:10.1002/cnm.1630050609.

[36] C. Strangfeld, S. Johann, M. Müller, M. Bartholmai, Embedded passive RFID-based sensors for moisture monitoring in concrete, in: IEEE Sensors, IEEE, 2017, pp. 1–3. doi:10.1109/ICSENS.2017.8234166.